BSM HIGGS SEARCHES WITH THE ATLAS EXPERIMENT*

Marco Schioppa

on behalf of the ATLAS Collaboration

Universitá della Calabria/INFN
via Pietro Bucci, 87036 Arcavacata di Rende, Cs, Italy

(Received April 25, 2016)

The searches for evidence of beyond the Standard Model (BSM) Higgs bosons is a crucial part of the LHC physics program. These searches are mainly driven by two approaches: directly from decays of neutral and charged Higgs bosons, indirectly by interpreting measured mass and couplings of light Higgs boson in extensions of the SM. This note reviews the most recent BSM Higgs boson searches performed with ATLAS at the LHC using Run 1 and early Run 2 proton–proton collision data. In particular, limits on new phenomena via coupling measurements, searches for charged and neutral Higgs bosons, double Higgs boson production and scalar particles decaying to $\gamma\gamma$ are presented. No significant deviations from the SM background expectations are found in any of the searches and thus the resulting exclusion limits are given.

DOI:10.5506/APhysPolB.47.1565

1. Introduction

The observation of a new particle with mass $m_H = 125.09^{\pm 0.21(\text{stat})}_{\pm 0.11(\text{syst})}$ GeV at the LHC [1] is a striking success for the Standard Model (SM) mechanism for electroweak symmetry breaking [2–7]. At present, the measurements of the production and decay modes of this particle indicate that it is compatible with the long-sought Standard Model (SM) Higgs boson. Nevertheless, more data and measurements are needed to extract reliable conclusions. The unexplained phenomena and problems, such as the nature of dark matter and dark energy, matter–antimatter asymmetry, neutrino oscillations, inconsistency with the general relativity and hierarchy problem, suggest us

* Presented at the Cracow Epiphany Conference on the Physics in LHC Run 2, Kraków, Poland, January 7–9, 2016.

that the SM must be embedded within a more complete theoretical model. Many such BSM models predict the existence of more than one Higgs boson. In a generic Two-Higgs Doublet Model (2HDM), there are two electroweak doublets, in contrast to the one doublet of the SM [8]. These models introduce five Higgs bosons (A, h, H, $H^{\pm}$), where A is a neutral pseudoscalar, h and H are neutral scalars, and $H^{\pm}$ are charged scalars. The Minimal Supersymmetric Standard Model (MSSM) [9–12] is a particular case of a 2HDM. The MSSM, as well as other 2HDMs, are compatible with existing measurements, including the recently discovered Higgs boson [13, 14]. In addition to introducing new particles, the extensions of the SM scalar sector may affect the properties of the SM-like Higgs boson discovered at the LHC. Enhancement of rare decays, completely new decays and production mechanisms, and different couplings with respect to the SM expectations are possible and may indicate connections to other puzzles, such as dark matter. The ATLAS experiment [15] at the Large Hadron Collider (LHC) has run extensive physics searches to cover as many scenarios as possible.

This proceeding review a selection of results among the many searches for BSM Higgs boson signatures based on the LHC proton–proton collision data collected in Run 1 at $\sqrt{s} = 7$ and 8 TeV and in the first year of Run 2 at $\sqrt{s} = 13$ TeV. In particular, limits on new phenomena via coupling measurements, searches for charged Higgs bosons and double Higgs boson production refer to Run 1 data taking, while the searches for neutral Higgs bosons production decaying to $\tau\tau$ and that of scalar particles decaying to $\gamma\gamma$ refer to the Run 2 data taking. No significant deviations from the SM background expectations are found in any of the searches and thus the resulting exclusion limits are given.

2. ATLAS detector and data taking

The ATLAS detector [15] consists of four major parts: the Inner Detector to track precisely charged particles and reconstruct common vertices; the Calorimeter system to measure the energy of easily stopped particles; the muon system to make additional standalone measurements of highly penetrating muons; the two magnet systems to bend charged particles in the Inner Detector and in the Muon Spectrometer, allowing their momenta to be measured.

The detector operates with close to 100% efficiency and provides performance characteristics slightly better than its design values. A three-level trigger system provides information to identify, in real time, the most interesting events to retain for detailed analysis. Figure 1 shows the total integrated luminosity recorded in 2011 ($\sqrt{s} = 7$ TeV) and 2012 ($\sqrt{s} = 8$ TeV) (left) and that recorded in 2015 ($\sqrt{s} = 13$ TeV) (right).

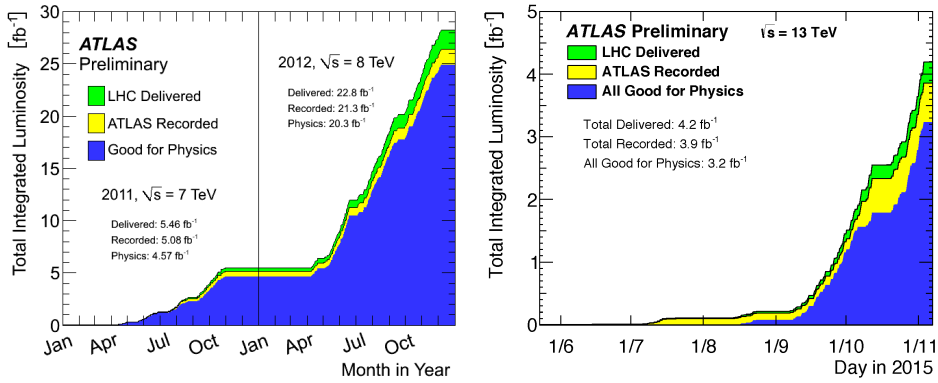

Fig. 1. (Color online) Delivered (gray/green), recorded (light gray/yellow) and "good for physics" (black/blue) integrated luminosity as a function of time during stable beams and for p–p collisions at $\sqrt{7}$ and $\sqrt{8}$ TeV in 2011 and 2012 (left) and at $\sqrt{13}$ TeV in 2015 (right). Taken from [16, 17].

3. Limits on new phenomena

The ATLAS experiment at the LHC has measured [18], with up to 4.7 fb^{-1} of p–p collision data at $\sqrt{s} = 7$ TeV and 20.3 fb^{-1} at $\sqrt{s} = 8$ TeV, couplings in the following visible Higgs boson decay channels: $h \to \gamma\gamma$, $h \to ZZ^* \to 4\ell$, $h \to WW^* \to \ell\nu\ell\nu$, $h \to Z\gamma$, $h \to bb$, $h \to \tau\tau$ and $h \to \mu\mu$ ($\ell = e, \mu$). Search results from tth associated production with $h \to \gamma\gamma$, $h \to bb$, and final states with multiple leptons are included. In addition, the constraints on the Higgs boson invisible decay branching ratio use direct searches for Higgs boson decays to invisible particles in events with dileptons or dijets with large missing transverse momentum ($E_{\mathrm{T}}^{\mathrm{miss}}$) such as the events from vector boson fusion (VBF) that produces $jjh(h \to E_{\mathrm{T}}^{\mathrm{miss}})$, and those from $Zh \to \ell\ell h(h \to E_{\mathrm{T}}^{\mathrm{miss}})$ and $W/Zh \to jjh(h \to E_{\mathrm{T}}^{\mathrm{miss}})$.

Each measurement or search classifies candidate events into exclusive categories based on the expected kinematic properties of different Higgs boson production processes. This improves the sensitivity and enables discrimination between different Higgs boson production modes. Each search channel is designed to be mostly sensitive to the product of a Higgs boson production cross section and decay branching ratio. The combination of the visible decay search channels is used to determine the couplings of the Higgs boson to other SM particles. In the benchmark models considered, the couplings of the Higgs boson to fermions and vector bosons are modified by functions of the model parameters. In all cases, it is assumed that the modifications of the couplings do not change the Higgs boson production or decay kinematics significantly. Thus, the expected rate of any given process can be obtained through a simple rescaling of the SM couplings and no acceptance change due to kinematics in each BSM scenario is included.

Deviations from the rates of Higgs boson production and decay predicted by the SM, including both the visible and invisible decay channels, have been searched for. Simultaneous fits of multiple production and decay channels are performed after the removal of overlaps in the event selection of different analyses, and correlations between the systematic uncertainties are accounted for. The data are interpreted in various benchmark models BSM, providing indirect limits on the BSM parameters. The limits make different assumptions than those obtained by direct searches for heavy Higgs bosons and invisible Higgs boson decays.

Limits are set on parameters in extensions of the Standard Model including a composite Higgs boson. Together with the measured mass of the scalar Higgs boson in the $\gamma\gamma$ and ZZ decay modes, a lower limit is set on the pseudoscalar Higgs boson mass of $m_A > 370$ GeV in the Minimal Supersymmetric Standard Model in which the mass of the neutral CP-even Higgs bosons h is set to that of the observed particle [19] (this model is known as the simplified MSSM or hMSSM). Results from direct searches for heavy Higgs bosons are also interpreted in the hMSSM.

The mass dependence of the couplings is consistent with the predictions for an SM Higgs boson. Constraints are set on Minimal Composite Higgs Models, models with an additional electroweak singlet, and Two-Higgs Doublet Models.

Contours of the two-dimensional likelihood in the plane of the parameters m_A and $\tan\beta$ (defined as the ratio of the vacuum expectation values of the two Higgs doublets and the mixing angle α between the CP-even Higgs bosons) for the hMSSM model are shown in Fig. 2. The data are consistent with the SM decoupling limit at large m_A. The observed (expected) lower limit at the 95% C.L. on the CP-odd Higgs boson mass is at least $m_A > 370$ GeV (310 GeV) for $1 < \tan\beta < 50$, increasing to 440 GeV (330 GeV) for $\tan\beta = 1$. The observed limit is stronger than expected because the measured rates in the $h \to \gamma\gamma$ (expected to be dominated by a W boson loop in the SM) and $h \to ZZ \to 4\ell$ channels are higher than predicted by the SM, but the hMSSM model has a physical boundary that implies the vector boson coupling (k_{V}) cannot be larger than the SM value. The physical boundary is accounted for by computing the profile likelihood ratio with respect to the maximum likelihood obtained within the physical region of the parameter space, $m_A > 0$ and $\tan\beta > 0$. For $\tan\beta < 1$, the couplings to SM particles receive potentially large corrections related to the top sector that have not been included.

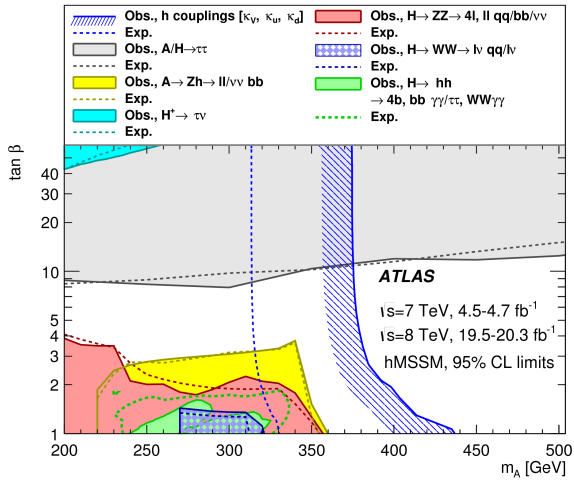

Fig. 2. Regions of the $[m_A, \tan\beta]$ plane excluded in the hMSSM model via fits to the measured rates of Higgs boson production and decays. The likelihood contours where $-2\ln\Lambda = 6.0$, corresponding approximately to the 95% C.L. (2 std. dev.), are indicated for the data and expectation for the SM Higgs sector. Taken from [18].

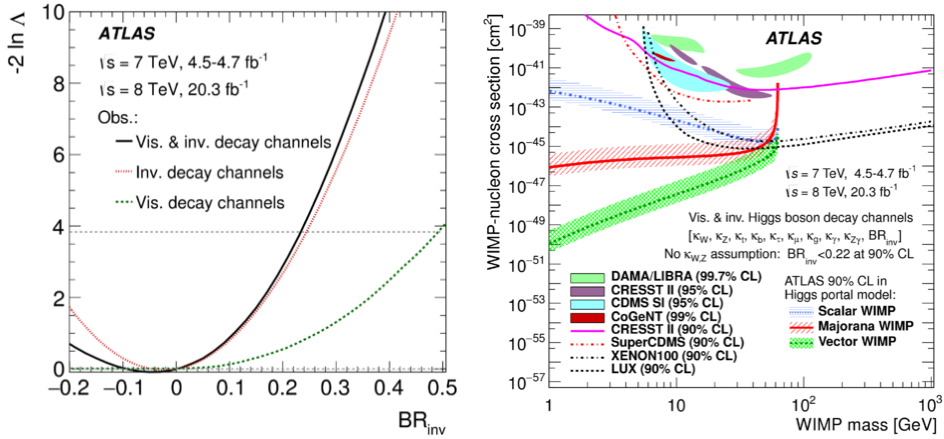

Fig. 3. (Color online) Left: Observed likelihood scans of the Higgs boson invisible decay branching ratio. The dashed (red) line and the dotted (green) line correspond to the direct searches for invisible and visible Higgs boson decays, respectively. The solid black line instead is the overall combination of these two decay channels. Right: Upper limit at the 90% C.L. on the WIMP-nucleon scattering cross section in a Higgs portal model as a function of the mass of the dark-matter particle. Excluded and allowed regions from direct detection experiments are also shown. Taken from [18].

Astrophysical observations provide strong evidence of dark matter that could be explained by the existence of weakly interacting massive particles (WIMPS) [20]. If such decays are kinematically allowed, the observed Higgs boson might decay to dark matter or other stable or long-lived particles which do not interact significantly with a detector. Such invisible decays of Higgs bosons can be inferred indirectly through final states with large missing transverse momentum. The direct searches for invisible Higgs boson decays in the vector boson fusion and associated production of a Higgs boson with W/Z ($Z \to \ell\ell$, $W/Z \to \jmath\jmath$) modes are statistically combined to set an upper bound at the 95% C.L. on the Higgs boson invisible decay branching ratio of 0.25. The use of the measured visible decay rates in a more general coupling fit improves the upper limit to 0.23, as shown in Fig. 3 (left). The limit on the invisible decay branching ratio is used to constrain the rate of dark matter–nucleon scattering in a model with a Higgs portal to dark matter. The results are summarized in Fig. 3 (right).

4. Search for $H^{\pm} \to tb$

Charged scalar Higgs boson indicate clearly physics BSM. They are predicted by several non-minimal Higgs scenarios, such as 2HDM [21] and models containing Higgs triplets [22]. The production mechanisms and decay modes of a charged Higgs boson depend on its mass ($m_{H^{\pm}}$) . If $m_{H^{\pm}} < m_{\text{top}}$, the primary production mechanism is $t \to bH^{\pm}$. For $m_{H^{\pm}} > m_{\text{top}}$, the dominant $H^{\pm}$ production mode at the LHC is expected to be in association with a top quark: $H^{\pm} \to tb$ with a substantial contribution from the $\nu\tau$ channel for large values of $\tan\beta$. A complementary $H^{\pm}$ production mode is the s-channel process $qq' \to H^{\pm}$.

The search for a charged Higgs boson presented here [23] is based on 20.3 fb^{-1} integrated luminosity of p–p collision data collected by ATLAS during Run 1 at $\sqrt{s} = 8$ TeV. In the production mode in association with a top quark, $gb \to tH^{+}$ with $H^{+} \to tb$, the top quarks both decay via $t \to Wb$, where one W boson decays hadronically and the other decays into an electron or a muon, either directly or through a τ-lepton decay, and the corresponding neutrino(s). The signal event signature is, therefore, characterized by the presence of exactly one high-p_{T} charged lepton (electron or muon) and five or more jets, at least three of them being b-tagged. A total of five independent categories are considered: four control regions (CR) with little sensitivity to signal, $4\jmath(2b)$, $5\jmath(2b)$, $\geq 6\jmath(2b)$, $4\jmath(\geq 3b)$, and one signal-rich region (SR), $\geq 5\jmath(\geq 3b)$. The SM backgrounds in each category are summarized in Fig. 4 (left). The dominant background process in every category is the production of $t\bar{t}$ pairs with additional jets in the final state. In all categories except $\geq 6\jmath(2b)$, the data exceed the SM prediction, but

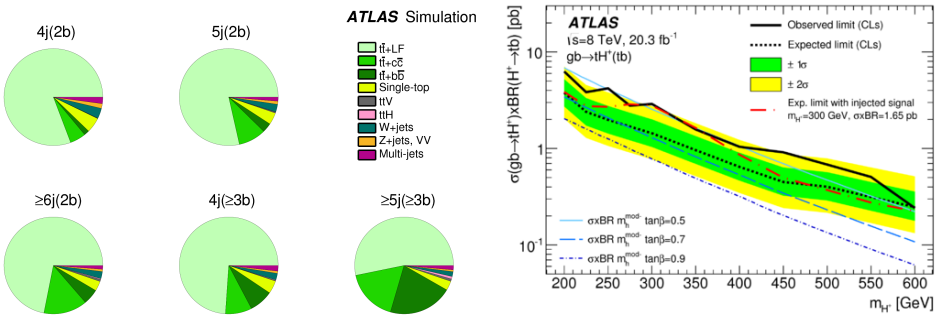

Fig. 4. (Color online) Left: Expected proportions of background processes in each of the signal-depleted and signal-rich regions in the search for a charged Higgs boson produced in association with a top quark. Taken from [24]. Right: Expected and observed limits for the production of $H^+ \to tb$ in association with a top quark. Theory predictions are shown for three representative values of $\tan\beta$ in the m_{mod}^- benchmark scenario of the MSSM [25]. Taken from [23].

they are consistent within the large uncertainties on the background. The 95% confidence level (C.L.) upper limits on $\sigma(gb \to tH^+) \times \text{BR}(H^+ \to tb)$ are presented in Fig. 4 (right). At $m_{H^+} = 300$ GeV, the excess of the data with respect to the background-only hypothesis corresponds to 2.3 standard deviations. The dash-dotted (red) line corresponds to the expected limit obtained in the case where a simulated signal is injected at $m_{H^+} = 300$ GeV, with a production cross section times branching fraction of 1.65 pb.

The search for $H^+ \to tb$ produced in the s-channel (*i.e.* via $qq' \to H^+$, the most commonly occurring reaction is $cs \to H^+$) is based on final states with one charged lepton (electron or muon) and jets, or hadronic jets only. In the search for $H^+ \to tb \to (\ell\nu b)b$, where the charged lepton ℓ is an electron or muon, only events collected with exactly one charged lepton plus two or three jets (two of them b-tagged) are required. In the search for $H^+ \to tb \to (qq'b)b$, the final state is characterized by hadrons: only one top-tagged jet (a jet substructure technique is used to reconstruct the top-quark decay products in one single large-radius jet) and only one b-tagged jet. Events with isolated charged leptons are vetoed in the event selection.

No significant excess of data with respect to the SM predictions is observed in the s-channel selected samples, as illustrated in Fig. 5.

For the lepton+jets (all-hadronic) final state and the charged Higgs boson mass range of 0.4–2.0 TeV (1.5–3.0 TeV), these observed upper limits lie between 0.13 and 6.7 pb (0.09 and 0.22 pb). The corresponding expected upper limits on the cross section times branching fraction are 0.18–7.4 pb (0.11–0.21 pb). The two s-channel analyses are reinterpretations of recent searches for $W' \to tb$ in ATLAS [26, 27].

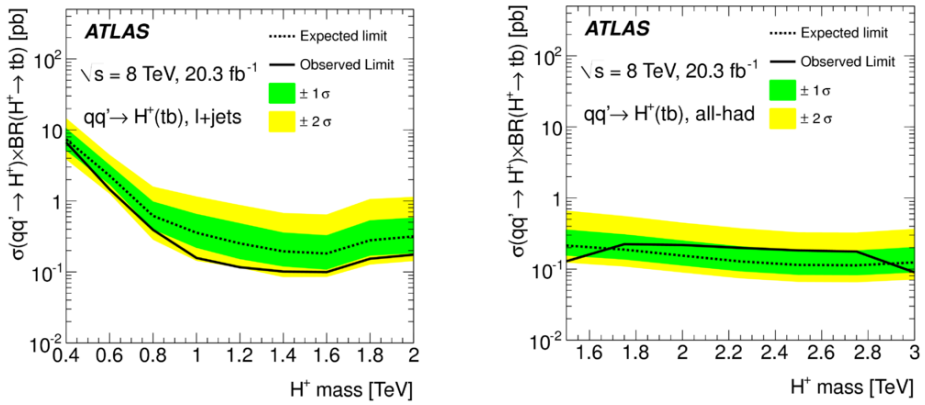

Fig. 5. Expected and observed 95% C.L. limits on the s-channel production cross section times branching fraction for $H^+ \to tb$ as a function of the charged Higgs boson mass, in the (left) lepton+jets final state and (right) all-hadronic final state, including all systematic uncertainties, using a narrow-width approximation. Taken from [23].

5. Search for $H/A \to \tau^+\tau^-$

The couplings of the MSSM heavy Higgs bosons to down-type fermions are enhanced with respect to the SM for large $\tan\beta$ values resulting in increased branching fractions to τ leptons and b quarks, as well as a higher cross section for Higgs boson production in association with b quarks. This has motivated the search for neutral MSSM Higgs bosons in $\tau\tau$ final states [28] performed using 3.2 fb^{-1} of p–p collisions collected by ATLAS in 2015 at $\sqrt{s} = 13$ TeV, that improves the limits of the previous ATLAS analysis [29, 30]. The heavy resonance produced via gluon fusion or b-associated production is assumed to decay to a $\tau^+\tau^-$ pair. The search considers the $\tau_{\text{had}}\tau_{\text{had}}$ and $\tau_{\text{lep}}\tau_{\text{had}}$ decay mode, where the τ_{lep} represents the decay of a τ to an electron or a muon, and neutrinos and τ_{had} the decay to hadrons and neutrino. The $H/A \to \tau_{\text{had}}\tau_{\text{had}}$ signal event selection requires exactly two back-to-back τ_{had} ($\phi > 2.7$ rad) with the opposite sign electric charge and a veto on electron and muon. The selection of $\tau_{\text{lep}}\tau_{\text{had}}$ events instead requires only one τ_{had} candidate and only one lepton (e or μ) with zero total charge. In addition, to reduce the SM backgrounds with little signal loss, further conditions are imposed: $|\phi_{\tau_{\text{had}}} - \phi_\ell| > 2.4$ rad, the transverse mass $m_{\text{T}}(\ell, E_{\text{T}}^{\text{miss}})$ outside the interval [40–150] GeV and the invariant mass of the electron and the τ_{had} must lie outside the interval [80–110] GeV.

As discriminating variable to achieve a good signal and background separation, the di-tau mass reconstruction is employed. The algorithm used for both the $\tau_{\text{had}}\tau_{\text{had}}$ and $\tau_{\text{lep}}\tau_{\text{had}}$ channels defines the total transverse mass

as: $m_{\mathrm{T}}^{\mathrm{tot}} = \sqrt{m_{\mathrm{T}}^2(E_{\mathrm{T}}^{\mathrm{miss}}, \tau_1) + m_{\mathrm{T}}^2(E_{\mathrm{T}}^{\mathrm{miss}}, \tau_2) + m_{\mathrm{T}}^2(\tau_1, \tau_2)}$. The $m_{\mathrm{T}}^{\mathrm{tot}}$ mass distributions for $\tau_\mu \tau_{\mathrm{had}}$ and $\tau_{\mathrm{had}}\tau_{\mathrm{had}}$ are shown in Fig. 6. In all considered cases, the observed event yields are found to be, within uncertainties, in good agreement with the predicted SM background yields and hence the

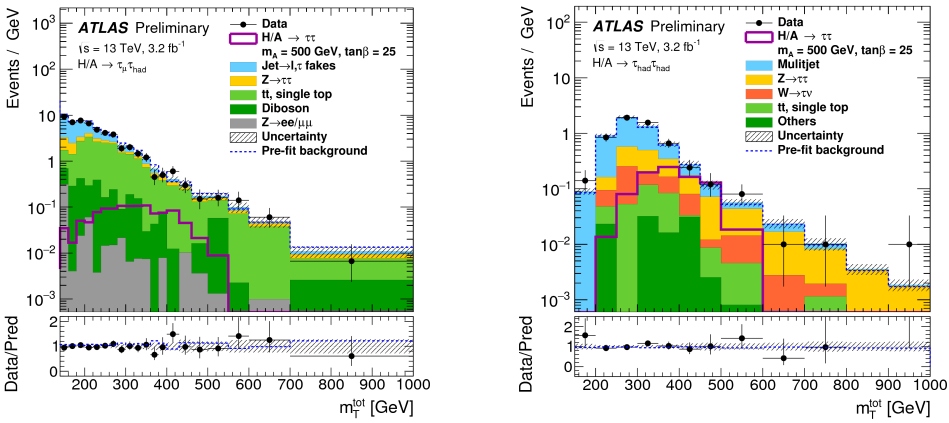

Fig. 6. The $m_{\mathrm{T}}^{\mathrm{tot}}$ distribution for the channels $\tau_\mu \tau_{\mathrm{had}}$ (left) and $\tau_{\mathrm{had}}\tau_{\mathrm{had}}$ (right), after the full selection. The data are compared to the background expectation and a hypothetical MSSM signal ($m_A = 500$ GeV and $\tan\beta = 25$). The background uncertainty includes statistical and systematic uncertainties. Taken from [28].

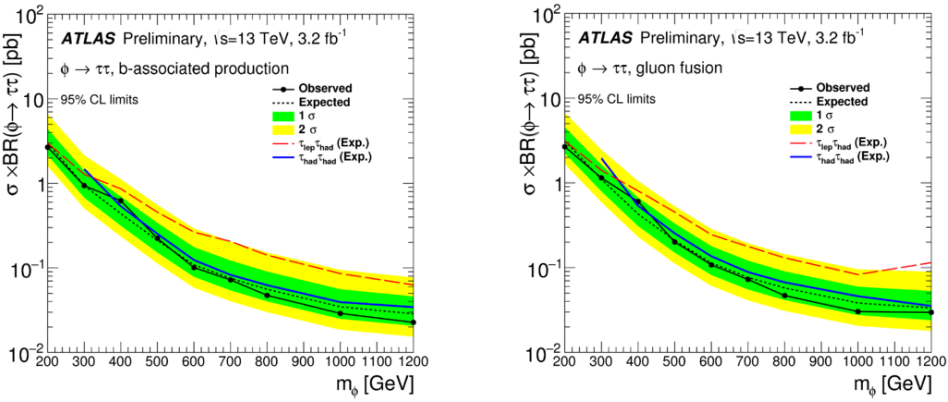

Fig. 7. The expected and observed 95% C.L. upper limits on the production cross section of a scalar particle Φ times branching ratio $\Phi \to \tau\tau$ for the combination of the $\tau_\ell \tau_{\mathrm{had}}$ and $\tau_{\mathrm{had}}\tau_{\mathrm{had}}$ channels. The production mechanism is assumed to be gluon fusion (left) and b-associated production (right). For comparison, the expected limits for the individual channels, $\tau_\ell \tau_{\mathrm{had}}$ and $\tau_{\mathrm{had}}\tau_{\mathrm{had}}$, are shown as well. Taken from [28].

results are given in terms of upper limits on the production cross section times branching fraction of a scalar boson as a function of its mass. The results from the channels studied in this search are combined to improve the sensitivity to MSSM Higgs boson production. Figure 7 shows the 95% upper limits for the combination of the $\tau_{\text{lep}}\tau_{\text{had}}$ and $\tau_{\text{had}}\tau_{\text{had}}$ channels for the gluon fusion production (left) and b-associated production (right) mechanisms. The results are interpreted in a range of MSSM scenarios. The most stringent constraints on $\tan\beta$ for the search excludes $\tan\beta > 10$ for $m_A = 200$ GeV.

6. Search for $hh \to bb\tau\tau, \gamma\gamma WW^*, \gamma\gamma bb, bbbb$

The Standard Model predicts two mechanisms for Higgs boson pair production (named non-resonant production processes): self-coupling between Higgs bosons and the Higgs-fermion Yukawa interactions. It is general opinion [31, 32] that the data collected so far (≈ 25 fb^{-1}) are insensitive to the self-coupling in the SM, because of the expected small signal and large backgrounds. Moreover, physics BSM can potentially enhance the production rate due to the resonant decay of a MSSM heavy CP-even neutral Higgs boson H [33] or even in a non-resonant way predicted by the CHBM [14].

The searches performed by ATLAS using 20.3 fb^{-1} of $\sqrt{s} = 8$ TeV p–p collision data refer to four final states: $hh \to \gamma\gamma bb$ [34], $bbbb$ [35], $bb\tau\tau$ [36], $\gamma\gamma WW^*$ [36]. Both resonant and non-resonant anomalous production of hh pairs is searched for. At the mass value of the new discovered particle h ($m_h = 125.4$ GeV), the SM predicts the following values for the decay fractions of $hh \to bbbb, bb\tau\tau, \gamma\gamma bb, \gamma\gamma WW^*$: 32.6%, 7.1%, 0.26% and 0.10%, respectively.

The $hh \to \gamma\gamma bb$ analysis requires two isolated photons with di-photon invariant mass $105 < m_{\gamma\gamma} < 160$ GeV and two b-tagged jets with dijet mass $95 < m_{bb} < 135$ GeV. For both resonant and non-resonant analysis, the 95% C.L. upper limits on the production of a narrow-width heavy scalar boson decaying to hh as a function of its mass are computed. For the non-resonant analysis, the upper limit is 2.2(1.0) pb for the observed (expected) cross section $\sigma(gg \to hh \to \gamma\gamma bb)$. For the resonant analysis, the upper limits observed (expected) on $\sigma(gg \to H) \times \text{BR}(H \to hh)$ are 2.3 (1.7) pb at $m_H = 260$ GeV and 0.7 (0.7) pb at $m_H = 500$ GeV. The global probability of an excess as significant as the observation to occur at any mass in the range studied is found to be 0.019, corresponding to 2.1 standard deviations. The results for the resonant case is shown in Fig. 8 (left).

The $hh \to bbbb$ analysis benefits from the largest $\text{BR}(h \to bb)$. The analysis attempts to reconstruct and identify separate b-quark jets from the $h \to bb$ decay (resolved method). Two back-to-back and high-momentum bb

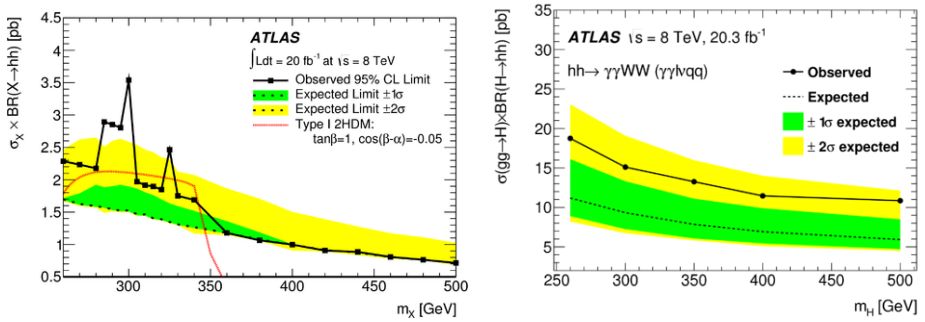

Fig. 8. The observed and expected upper limit at 95% C.L. on the $\sigma(gg \to X) \times \mathrm{BR}(X \to hh)$ as a function of m_X from the resonant $\gamma\gamma bb$ analysis (left) and on $\sigma(gg \to H) \times \mathrm{BR}(H \to hh)$ as a function of m_H from the resonant $hh \to \gamma\gamma WW^*$ analyses (right). Taken from [34, 36].

systems with their masses consistent with m_h are searched for. For the non-resonant search, both the observed and expected 95% C.L. upper limit on the $\sigma(pp \to hh \to bbbb)$ is 202 fb. For the resonant search, the invariant mass of the four jets is used as the final discriminant from which the upper limit on the potential signal cross section is extracted. The resulting observed (expected) 95% C.L. upper limit on $\sigma(pp \to H \to hh \to bbbb)$ ranges from 52 (56) fb, at $m_H = 500$ GeV, to 3.6 (5.8) fb, at $m_H = 1000$ GeV.

In the $hh \to bb\tau\tau$ decay channel, the final state with one τ lepton decaying hadronically and the other one decaying leptonically with zero total electric charge is used. Moreover, the candidate $bb\ell\tau_{\mathrm{had}}$ events must have $p_{\mathrm{T}}^{\ell} > 20$ GeV and two or more jets with $p_{\mathrm{T}}^{\mathrm{jet}} > 30$ GeV, some of which b-tagged. For the non-resonant search, the observed di-tau invariant mass distribution agrees well with that of the estimated background events. For the resonant search, a small deficit with a local significance of approximately 2σ is observed in the data relative to the background expectation at $m_{bb\tau\tau} \sim 300$ GeV. No evidence of Higgs boson pair production is present in the data.

In the $hh \to \gamma\gamma WW^*$ decay channel, one Higgs boson decays to a pair of photons and the other decays to a pair of W bosons. To reduce multijet backgrounds, one of the W bosons is required to decay leptonically (e/μ either directly or through a τ lepton), whereas the other is required to decay hadronically, leading to the $\gamma\gamma\ell\nu qq$ final state. Events are required to have $\geq 2\gamma$ with $|m_{\gamma\gamma} - m_h| < 3.4$ GeV for the $h \to \gamma\gamma$ and ≥ 2 jets, only one e/μ, $E_{\mathrm{T}}^{\mathrm{miss}}$ and no b-tagged jets for the $h \to WW^*$. For the resonant production, limits are set on the $\sigma(gg \to H) \times \mathrm{BR}(H \to hh)$ as a function of m_H. The observed (expected) limits of the $hh \to \gamma\gamma WW^*$ analyses are illustrated in Fig. 8 (right).

The results of the four analyses are first determined separately and then combined together. The most significant excess in the combined results is at a resonance mass of 300 GeV with a local significance of 2.5σ, largely due to the 3.0σ excess observed in the $hh \to \gamma\gamma bb$ analysis. The upper limit on $\sigma(gg \to H) \times \mathrm{BR}(H \to hh)$ varies from 2.1 pb at 260 GeV to 0.011 pb at 1000 GeV. These limits are shown in Fig. 9 (left) as a function of m_H. The improvement above $m_H = 500$ GeV is due to the sensitivity of the $hh \to bbbb$ analysis. The upper cross-section limits of the resonant search are also interpreted in the context of the hMSSM scenario as exclusion regions in the $(\tan\beta, m_A)$ plane as illustrated in Fig. 9 (right). The improved sensitivity in the expected exclusion on the contour line of $m_H \sim 260$ GeV reflects the improved expected limit on the cross section.

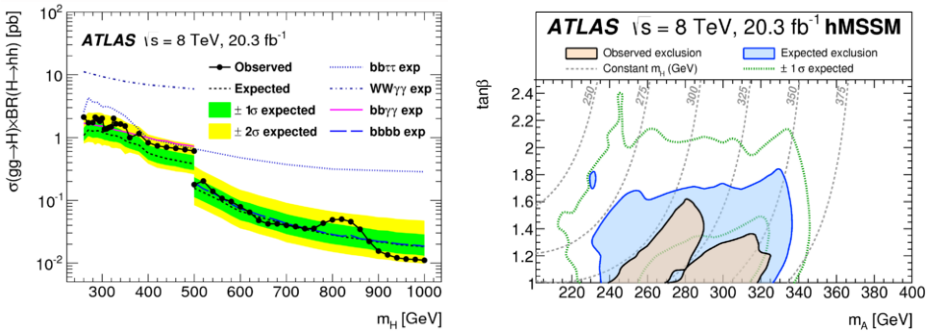

Fig. 9. Left: The observed and expected 95% C.L. upper limits on $\sigma(gg \to X) \times \mathrm{BR}(X \to hh)$ as a function of m_H, combining resonant searches in $hh \to \gamma\gamma bb$, $bbbb$, $bb\tau\tau$ and $\gamma\gamma WW^*$ final states. Right: The observed and expected 95% C.L. exclusion regions in the $(\tan\beta, m_A)$ plane of MSSM scenarios from the resonant search in the hMSSM scenario. The gray dashed lines show the constant values of the heavy CP-even Higgs boson mass. Taken from [36].

7. Resonances decaying to photon pairs

ATLAS has searched for new resonances decaying to $\gamma\gamma$ pairs with invariant mass larger than 200 GeV, such as those expected in models with an extended Higgs sector, using both 20.3 fb^{-1} and 3.2 fb^{-1} p–p collisions data collected at $\sqrt{s} = 8$ TeV and 13 TeV, respectively [38, 39]. Additional Higgs-like resonances are expected to manifest themselves as localized excesses of events in the reconstructed di-photon invariant mass distribution over a large, smooth background. The analysis selects pairs of photons using tight identification criteria to minimize backgrounds other than direct SM di-photon production. The total signal selection efficiency ranges from 25 to 40% depending on the boson production mechanism (ggF, VBF, ttH)

and on the resonance masses. Figure 10 (left) shows the di-photon invariant mass spectrum observed in data collected during Run 2. The data are consistent with the expected background in most of the mass range. The most significant deviation in the observed di-photon invariant mass spectrum is found around 750 GeV, with a global significance of about 2σ as shown in Fig. 10 (right). A limit is reported on the fiducial production cross section of a narrow scalar boson times its decay branching ratio into two photons, for masses ranging from 200 GeV to 1.7 TeV as shown in Fig. 11 (left).

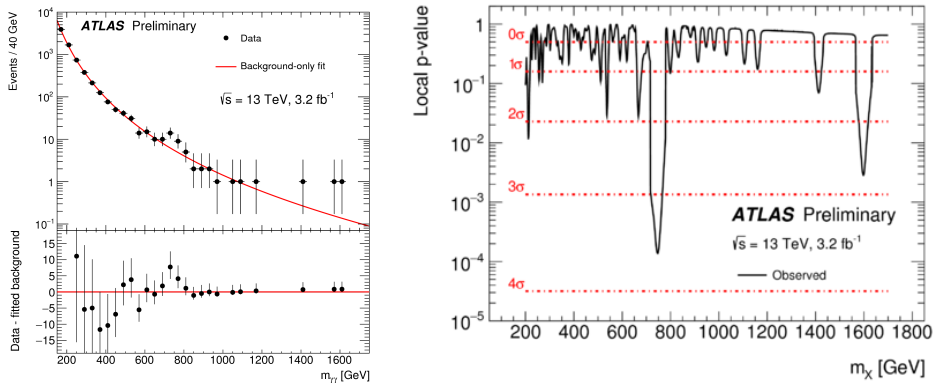

Fig. 10. Left: Invariant mass distribution of the selected di-photon events. Residual number of events with respect to the fit result are shown in the bottom pane. Right: p-value for the background-only hypothesis p_0 as a function of the mass m_X of a probed NWA resonance signal. Taken from [39].

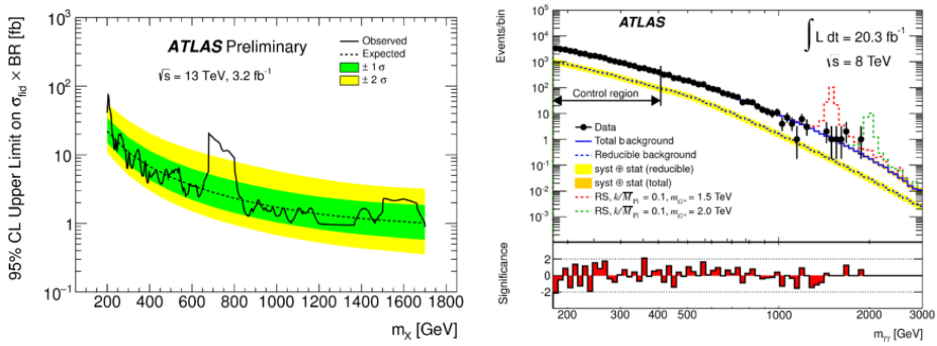

Fig. 11. Left: Expected and observed upper limits on $\sigma_{\text{fiducial}} \times \text{BR}(X \to \gamma\gamma)$ expressed at 95% C.L., as a function of the assumed value of the narrow-width scalar resonance mass m_X. Taken from [39]. Right: Observed di-photon invariant mass distribution with superimposed the SM background prediction. The bin-by-bin significance of the difference between data and background expectation is shown in the bottom panel. Taken from [40].

The excess of events around 750 GeV is scrutinized. No detector or reconstruction effect that could explain the larger rate is found, nor any indication of anomalous background contamination. The Run 1 analysis is extended to invariant masses larger than 600 GeV by using the new background modeling techniques. The compatibility between the results obtained with the 8 TeV and 13 TeV datasets is estimated under the Narrow Width Approximation (NWA) hypothesis. Figure 11 (right) shows the observed di-photon invariant mass using Run 1 data. For an s-channel gluon-initiated process, the parton-luminosity ratio is expected to be 4.7. Under those assumptions, the results obtained with the two datasets are found to be compatible in 2.2σ.

8. Conclusions

The search for beyond SM Higgs bosons is highly motivated and has just started having sensitivity to realistic scenarios. The discovery of a Higgs boson with mass around 125 GeV has opened new possibilities for searches, especially those that include the new particle in the final state. More data are needed in order to explore the possibility of an extended scalar sector and hence the community is looking forward to the new LHC run.

REFERENCES

[1] ATLAS Collaboration, CMS Collaboration, *Phys. Rev. Lett.* **114**, 191803 (2015) [arXiv:1503.07589 [hep-ex]].
[2] F. Englert, R. Brout, *Phys. Rev. Lett.* **13**, 321 (1964).
[3] P.W. Higgs, *Phys. Lett.* **12**, 132 (1964).
[4] P.W. Higgs, *Phys. Rev. Lett.* **13**, 508 (1964).
[5] G.S. Guralnik, C.R. Hagen, T.W.B. Kibble, *Phys. Rev. Lett.* **13**, 585 (1964).
[6] P.W. Higgs, *Phys. Rev.* **145**, 1156 (1966).
[7] T.W.B. Kibble, *Phys. Rev.* **155**, 1554 (1967).
[8] J.F. Gunion, H.E. Haber, G.L. Kane, S. Dawson, *The Higgs Hunter's Guide*, Frontiers in Physics, 2000, ISBN:0-7382-0305-X.
[9] P. Fayet, *Phys. Lett. B* **64**, 159 (1976).
[10] P. Fayet, *Phys. Lett. B* **69**, 489 (1977).
[11] G.R. Farrar, P. Fayet, *Phys. Lett. B* **76**, 575 (1978).
[12] P. Fayet, *Phys. Lett. B* **84**, 416 (1979).
[13] P. Bechtle *et al.*, *Eur. Phys. J. C* **73**, 2354 (2013) [arXiv:1211.1955 [hep-ph]].
[14] G.C. Branco *et al.*, *Phys. Rep.* **516**, 1 (2012) [arXiv:1106.0034 [hep-ph]].
[15] ATLAS Collaboration, *JINST* **3**, S08003 (2008).
[16] https://twiki.cern.ch/twiki/bin/view/AtlasPublic/LuminosityPublicResults

[17] https://twiki.cern.ch/twiki/bin/view/AtlasPublic/LuminosityPublicResultsRun2
[18] ATLAS Collaboration, *J. High Energy Phys.* **1511**, 206 (2015) [arXiv:1509.00672 [hep-ex]].
[19] L. Maiani, A.D. Polosa, V. Riquer, *Phys. Lett. B* **724**, 274 (2013) [arXiv:1305.2172 [hep-ph]].
[20] D. Clowe *et al.*, *Astrophys. J.* **648**, L109 (2006) [arXiv:astro-ph/0608407].
[21] T.D. Lee, *Phys. Rev. D* **8**, 1226 (1973).
[22] G. Lazarides, Q. Shafi, C. Wetterich, *Nucl. Phys. B* **181**, 287 (1981).
[23] ATLAS Collaboration, *J. High Energy Phys.* **1603**, 127 (2016) [arXiv:1512.03704 [hep-ex]].
[24] https://atlas.web.cern.ch/Atlas/GROUPS/PHYSICS/PAPERS/HIGG-2013-28/
[25] M. Carena *et al.*, *Eur. Phys. J. C* **73**, 2552 (2013) [arXiv:1302.7033 [hep-ph]].
[26] ATLAS Collaboration, *Phys. Lett. B* **743**, 235 (2015) [arXiv:1410.4103 [hep-ex]].
[27] ATLAS Collaboration, *Eur. Phys. J. C* **75**, 165 (2015) [arXiv:1408.0886 [hep-ex]].
[28] ATLAS Collaboration, ATLAS-CONF-2015-061, https://cds.cern.ch/record/2114827?ln=it
[29] ATLAS Collaboration, *J. High Energy Phys.* **1411**, 056 (2014) [arXiv:1409.6064 [hep-ex]].
[30] ATLAS Collaboration, *J. High Energy Phys.* **1302**, 095 (2013) [arXiv:1211.6956 [hep-ex]].
[31] U. Baur, T. Plehn, D.L. Rainwater, *Phys. Rev. D* **69**, 053004 (2004) [arXiv:hep-ph/0310056].
[32] M.J. Dolan, C. Englert, M. Spannowsky, *J. High Energy Phys.* **1210**, 112 (2012) [arXiv:1206.5001 [hep-ph]].
[33] H.E. Haber, G.L. Kane, *Phys. Rep.* **117**, 75 (1985).
[34] ATLAS Collaboration, *Phys. Rev. Lett.* **114**, 081802 (2015) [arXiv:1406.5053 [hep-ex]].
[35] ATLAS Collaboration, *Eur. Phys. J. C* **75**, 412 (2015) [arXiv:1506.00285 [hep-ex]].
[36] ATLAS Collaboration, *Phys. Rev. D* **92**, 092004 (2015) [arXiv:1509.04670 [hep-ex]].
[37] E. Bagnaschi *et al.*, LHCHXSWG-2015-002, 2015, http://cds.cern.ch/record/2039911
[38] ATLAS Collaboration, *Phys. Rev. Lett.* **113**, 171801 (2014) [arXiv:1407.6583 [hep-ex]].
[39] ATLAS Collaboration, ATLAS-CONF-2015-081, http://cds.cern.ch/record/2114853
[40] https://atlas.web.cern.ch/Atlas/GROUPS/PHYSICS/PAPERS/EXOT-2012-19/